

A Passive Heterodyne Hot Electron Bolometer Imager Operating at 850 GHz

Eyal Gerecht, *Member, IEEE*, Dazhen Gu, *Student Member, IEEE*, Lixing You, and K. Sigfrid Yngvesson, *Life Fellow, IEEE*

Abstract—We report on the development and characterization of a passive heterodyne hot electron bolometer (HEB) imager operating at 850 GHz. HEB detectors provide unprecedented sensitivity and spectral resolution at terahertz frequencies covering the frequency range of 0.5–5 THz. Terahertz imagers based on HEB technology have sufficient sensitivity to operate in a passive imaging mode, thus eliminating the need for active illumination. We demonstrated a fully automated passive imaging system based on our HEB technology. The front-end heterodyne detector includes a quasi-optically coupled HEB device in close proximity to a monolithic microwave integrated circuit low-noise IF amplifier. We integrated a compact commercial harmonic multiplier local oscillator (LO) source to provide the LO biasing for the HEB detector. Our high spectral resolution terahertz imager has a noise equivalent temperature difference value of 0.4 K and a spatial resolution of approximately 4 mm.

Index Terms—Heterodyne detection, hot electron bolometer (HEB) detectors, quasi-optical coupling, terahertz antennas, terahertz imaging.

I. INTRODUCTION

IMAGING AND spectroscopy at terahertz frequencies have great potential for healthcare, plasma diagnostics, and homeland security applications. Terahertz frequencies correspond to energy level transitions of important molecules in biology and astrophysics. Due to its shorter wavelength, terahertz radiation also offers higher spatial resolution than microwaves or millimeter waves.

Hot electron bolometer (HEB) mixer receivers for terahertz frequencies have been under development for astronomical applications over the past two decades [1]. HEBs are planar superconducting devices with extremely small parasitic reactances. The *TREND* spectroscopic instrument, which was deployed successfully at the South Pole in 2003 [2], is based on HEB technology.

We describe, in detail, the components and considerations involved in the development of a passive imaging system based on heterodyne detection operating at terahertz frequencies. We chose the atmospheric window centered on 850 GHz as the operational frequency of the imager in order to take advantage of the shorter wavelength when compared with millimeter-wave

imagers [3] for improved spatial resolution and a reduction in the size of the optical focusing elements. Images are formed by employing a mechanical scanner. Special attention was paid to the design of the data-acquisition system. We show in this discussion that the system can potentially acquire a 40×40 pixel image in approximately 8 s, sufficient for medical imaging. Other applications that require real time imaging can be implemented in future study by employing a focal plane array (FPA) of detectors of the type described here. A number of images designed to determine the thermal and spatial resolutions of the overall system were recorded and analyzed.

We first briefly discuss and compare different terahertz heterodyne detectors in Section II. In Section III, we present a schematic of our imaging system and discuss in detail the design of its components, especially the design and performance of the quasi-optical coupling of the local oscillator (LO) source and the thermal source beams to the heterodyne detector. The measured performance of the imager is given in Section IV, where we discuss measurements of the stability of the system, as well as the thermal and spatial resolutions achieved on the object. Finally, we suggest future improvements to the system in Section V.

II. HETERODYNE DETECTORS FOR TERAHERTZ FREQUENCIES

In this paper, we emphasize passive imaging of thermal objects at a temperature close to room temperature (300 K), and that emit radiation with a very low power on the order of 10^{-12} W (assuming a 1-GHz detection bandwidth). It is, therefore, of great importance to implement a detection technology with sufficient sensitivity. A heterodyne detector has superior sensitivity and spectral selectivity compared with a direct detector (except for direct detectors cooled to microkelvin temperatures that require much more complex cryogenics) and is the preferred choice for our terahertz imager.

The sensitivity of a heterodyne detection system is characterized by its system noise temperature. The distinction between system noise temperature and receiver noise temperature is that the former includes the noise from the input source, whereas the latter only includes the noise generated in the receiver.

Once the detector technology is chosen, the general architecture of the imager is determined. A general type of configuration used for microwave/terahertz radiometers involves switching of the input source in order to eliminate the effect of system gain fluctuations [4]. We chose a technique known as the Dicke receiver configuration [5], where the receiver collects the radiation signal and compares it with a known reference, usually a blackbody source with a well-controlled temperature, at a rate given by the switching frequency f_m . The output signal is then integrated for improved sensitivity while reducing the system susceptibility to gain fluctuations at the expense of scanning speed.

Manuscript received August 29, 2007; revised January 28, 2008.

E. Gerecht, D. Gu, and L. You are with the Electromagnetics Division, National Institute of Standards and Technology, Boulder, CO 80305 USA (e-mail: gerecht@nist.gov; dau@boulder.nist.gov; lyou@boulder.nist.gov).

K. S. Yngvesson is with the Department of Electrical and Computer Engineering, University of Massachusetts at Amherst, Amherst, MA 01003 USA (e-mail: yngvesson@ecs.umass.edu).

Color versions of one or more of the figures in this paper are available online at <http://ieeexplore.ieee.org>.

Digital Object Identifier 10.1109/TMTT.2008.921289

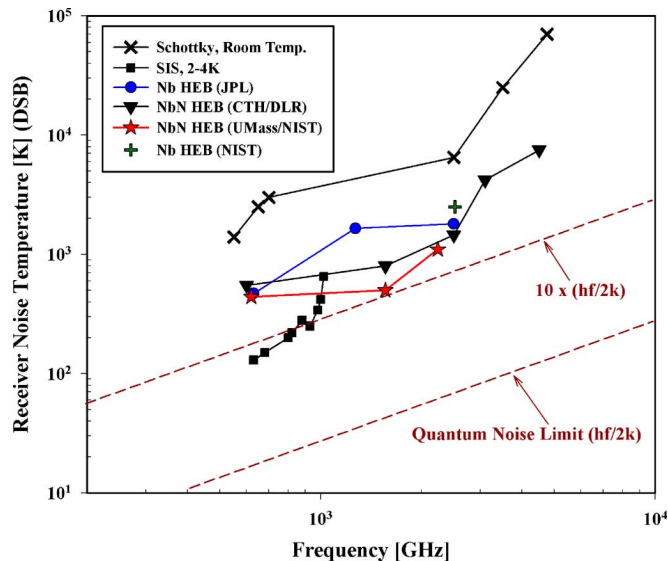


Fig. 1. DSB receiver noise temperature for different heterodyne receivers in the terahertz frequency range.

Three heterodyne detector technologies operating at terahertz frequencies exist today. The oldest and most developed is the Schottky-barrier diode (SBD) mixers [6]. These usually do not require cryogenic cooling. If designed with wide bandwidth, their sensitivity can be comparable with terahertz mixers made of superconducting materials. A passive imaging system at 640 GHz with an SBD mixer was described in [7]. SBD mixers have also been used in active imagers [8]. Such systems are possible at the higher terahertz frequencies thanks to the availability of higher power LO sources such as gas lasers or quantum cascade lasers (QCLs). This is because SBD mixers require LO power on the order of milliwatts when operated in the optimum region. Superconductor-insulator-superconductor (SIS) mixers have the best sensitivity up to and just above 1 THz, but are limited in frequency by the bandgap frequency ($2E_g/h$) of the superconductor material used for the SIS junction. HEB mixers exhibit sensitivities of close to ten times the quantum noise limit over the entire terahertz frequency range. We chose the HEB heterodyne detectors for our imager based on their having the lowest LO power consumption (a few hundred nanowatts) and their demonstrated ability to work in FPAs [9]. HEBs are also simpler to fabricate than SIS devices, and at 850 GHz, have an approximately comparable receiver noise temperature to SIS mixers. Fig. 1 illustrates the state-of-the-art double-sideband (DSB) receiver noise temperatures for different types of terahertz receivers over a broad frequency range. The quantum noise limit for the DSB system noise temperature is $hf/2k$ (shown by the lower dashed line in Fig. 1). The DSB receiver noise temperatures of the best receivers from 100 GHz to 2.5 THz approach the $10 \times hf/2k$ line (also shown by a dashed line).

At terahertz frequencies, there are currently a few choices of LO sources available, including far-infrared (FIR) lasers, harmonic multiplier sources, backward-wave oscillator (BWO) sources, and QCLs [10]. Harmonic frequency multiplier sources employ gallium-arsenide (GaAs) Schottky diodes. These sources are relatively compact, easy to use, and highly

tunable. The available output power decreases with increasing frequency. The best currently commercially available harmonic multiplier source,¹ operating at approximately 1.3 THz, can generate 10–12 μW of output power, which is sufficient to provide biasing power for a small number of detectors. Since our system frequency had been chosen to be 850 GHz, a harmonic multiplier source was the best choice for the LO source.

III. HEB-BASED IMAGING SYSTEM

The schematic diagram of a passive heterodyne imaging system at terahertz frequencies is illustrated in Fig. 2. The main components of such a system are the front-end detecting element (integrated mixer block), LO source, optics system, and data acquisition (DAQ) system. In order to produce a 2-D raster image, the heterodyne receiver collects radiation from the object through optical components, such as off-axis parabolic (OAP) mirrors and a thin Mylar beam splitter, while the target point is being scanned in both the elevation and azimuth directions. This signal beam is chopped against a room-temperature black-body source. The IF output signal from the mixer is amplified by a cryogenic low-noise amplifier (LNA) cascaded with a back-end IF chain of tunable gain and bandwidth operating at room temperature. The IF bandwidth of the receiver is limited by means of a bandpass filter, which is, in turn, connected to a standard microwave detector to produce a rectified voltage signal. This signal is then fed to a lock-in amplifier referenced by the chopping frequency. A dedicated DAQ system collects the lock-in amplifier's output signal as a function of position with respect to the target. Special considerations for system integration, signal processing, and scanning performance must be taken.

A. HEB Technology

HEBs are planar superconducting devices with extremely small parasitic reactance, even at the highest terahertz frequencies. HEB devices are able to absorb the terahertz radiation up to the visible range due to the very short momentum scattering times. HEBs change their resistance as the quasi-particles are heated as a function of the incoming energy. The quasi-particles within the HEB device absorb the radiation power and transfer the heat either through phonon interactions to the substrate, or through diffusion to the metal contacts [1]. The phonon-cooled HEB structure has been successfully deployed in astrophysical systems such as *TREND* [2] and developed for launch on *Herschel/Planck* [11]. Theoretical models of the physical behavior of the HEB device have been under development over the last decade. Such models include the simple point bolometer model [12] and the more advanced hot spot model [13].

The phonon-cooled HEB device is fabricated from an NbN film that has been sputtered onto a silicon substrate. The film thickness is typically 3.5–4 nm. Current HEB device dimensions are designed to be 2- μm wide and 0.5- μm long. The HEB device is connected at the terminals of a planar antenna, which is used for coupling the incoming radiation, as shown in Fig. 3. The device can be matched to the antenna by changing its aspect ratio. We have developed a relatively easy fabrication process

¹Virginia Diodes Inc., Charlottesville, VA, 2006. [Online]. Available: <http://www.virginiadiodes.com/multipliers.htm>

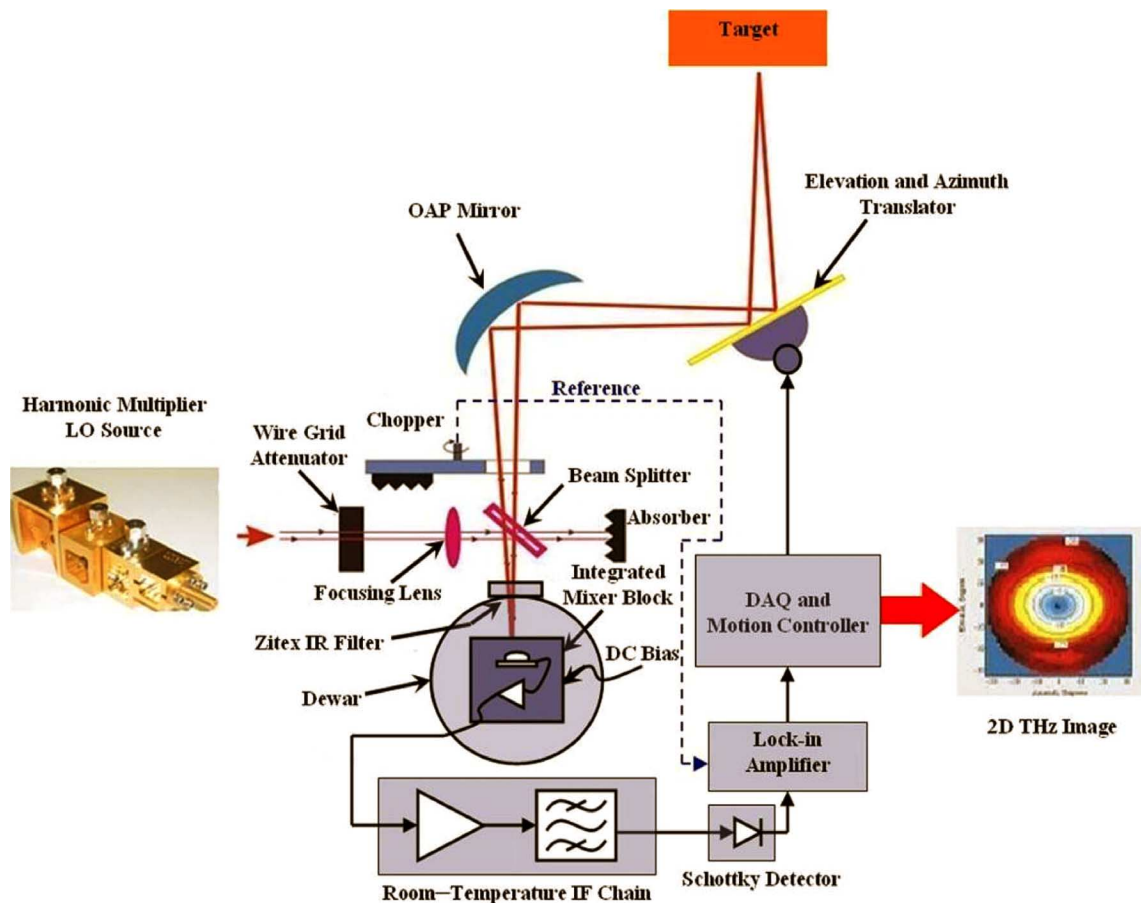


Fig. 2. Schematic of a 2-D terahertz passive imaging system.

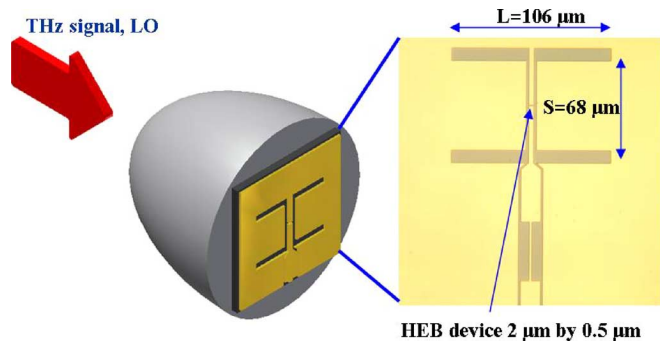


Fig. 3. Illustration of a quasi-optical system and a twin-slot antenna photograph.

based on UV lithographical techniques. A bi-layer liftoff step is performed to ensure a high yield fabrication process.

B. Terahertz Integrated Receiver

In a typical receiver system, the mixer and LNA are assembled in separate blocks and connected by coaxial cables. An isolator is often included between the mixer and LNA in order to minimize the standing wave between them. Although this configuration has been widely adopted in astrophysical receiver systems, it does not meet the requirement for a compact multipixel FPA. Furthermore, the use of isolators limits the IF bandwidth

to no more than an octave. In order to eliminate the use of isolators, we have developed a design that for the first time integrates the HEB device and the monolithic microwave integrated circuit (MMIC) LNA in the same block [14] (see Fig. 4). Earlier related work integrated SIS mixers and IF LNAs [15]–[18]. A multisection microstrip matching network is employed to achieve broadband coupling between the HEB and the MMIC LNA. The HEB device is located in close proximity to the MMIC chip, which is mounted in a narrow rectangular cavity for the purpose of eliminating possible amplifier oscillations. A three-stage MMIC HEMT amplifier fabricated on an InP substrate serves as the IF LNA, exhibiting remarkable noise performance over a wide frequency range [19]. This particular MMIC LNA has been characterized against standards developed at the National Institute of Standards and Technology (NIST), Boulder, CO, and, by use of a recently developed measurement technique [20], shown to exhibit noise temperatures below 5.5 K from 1 to 11 GHz. Fig. 4 shows a photograph of the HEB/MMIC integrated mixer block. To couple and monitor the dc bias to the device and extract the IF signal from the device, we use a bias “tee” circuit that is built into the mixer block.

C. LO Source

A commercially available 850-GHz harmonic multiplier source is employed as the LO signal. A phase-locked oscillator generates an output signal at 11.8 GHz. This signal is used to drive a multiplier chain, which is composed of one amplifier,

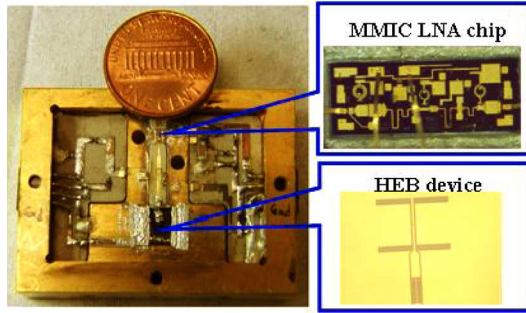


Fig. 4. Integrated mixer block housing an HEB device and an MMIC LNA.

two triplers, and three doublers. The terahertz signal injection is achieved by use of a WR 1.2 diagonal horn module assembled at the end of the multiplier chain. This particular harmonic multiplier source produces an output power of approximately $250 \mu\text{W}$. To combine the LO and signal beams, we employ a $25\text{-}\mu\text{m}$ -thick Mylar beam splitter that reflects 28% of the incoming LO radiation.

D. Quasi-Optical Coupling

To effectively couple the incoming LO and signal powers into the HEB mixer, we have designed a quasi-optical system consisting of a silicon lens and a monolithic antenna, and a number of focusing OAP mirrors.

1) *Printed Antenna in Combination With Dielectric Lens:* The majority of HEB receivers now use a quasi-optical coupling scheme for the incoming radiation by use of a combination of a dielectric lens and an integrated antenna. Waveguide coupling structures are also in use at the lower terahertz frequencies. A variety of printed antenna structures can be used to couple terahertz radiation into the HEB device.

We have employed two types of antennas: twin-slot antennas, which have a practical bandwidth of approximately 20%, and log-periodic antennas, which can be designed to have several octaves of bandwidth, depending on the number of teeth.

Fig. 5 shows the simulated reflection loss of a twin-slot antenna designed for 850 GHz. The minimum loss occurs at approximately 840 GHz and a relatively good match ($S_{11} < -10$ dB) is achieved within a frequency range of 720–930 GHz. The simulation includes the far-field radiation pattern radiated into the silicon lens. The twin-slot antenna has a highly symmetrical and linearly polarized radiation pattern and provides nearly perfect power coupling to an incident Gaussian beam [21].

The terahertz signals couple to the device through an elliptical silicon lens, 4 mm in diameter (Fig. 3). The lens is a rotational ellipsoid that functions as an aperture antenna, and hence, reshapes the far-field radiation pattern. By use of a ray-tracing technique, the radiation from the twin slot antenna, placed at the second focus of the lens, becomes a plane wave in the aperture plane outside the lens. The far-field beam, resulting from the silicon lens and the twin-slot antenna, has a full-width half-power (FWHP) of approximately 3° and a sidelobe level lower than -15 dB.

2) *Off-Axis Parabolic Mirrors:* Terahertz beam focusing components are needed in order to collect and reshape the radiation emitted from both the LO source and imaged object, and

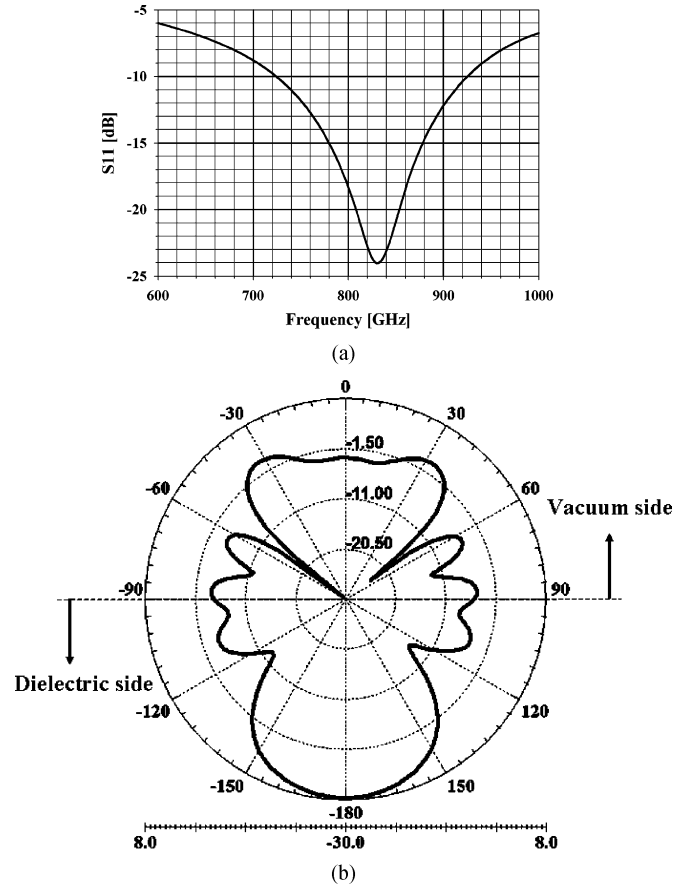


Fig. 5. Simulation of the: (a) reflection loss and (b) radiation pattern of the twin-slot antenna on a silicon substrate at 850 GHz.

direct them onto the antenna/lens structure. Terahertz lenses (that have some loss) or OAP mirrors can be used in a terahertz imaging system. OAP mirrors are free of chromatic aberrations and exhibit negligible loss, but require precise positioning and are known for producing higher order modes under the spill-over condition [22]. The contribution of the higher order modes to the reflected beam is given by the following equation based on a first-order approximation [22]:

$$E_r(x, y, z) \approx \left\{ 1 - \frac{U}{2} \cdot \left[2 \cdot \left| \frac{x}{w} \right| \cdot \left| \frac{4x^2}{w^2} - 3 \right| + \sqrt{2} \cdot \left| \frac{x}{w} \right| \cdot \left| \frac{4y^2}{w^2} - 1 \right| \right] \right\} \cdot E_{ri}(x, y, z) \quad (1)$$

where E_r is the distorted electric field, E_{ri} is the electric field distribution without higher order distortion, w is the beam radius, and U is the distortion factor, calculated as

$$U = \frac{w_m \cdot \tan \theta_i}{2\sqrt{2}f} \quad (2)$$

where w_m is the radius of the beam illuminated on the OAP mirror, θ_i is the beam incidence angle, and f is the focal length of the OAP mirror. The coordinate z is defined to be parallel to the optical axis for the reflected beam. Further, x is perpendicular to z in the plane of reflection, while y is perpendicular to z and x . To minimize the higher order mode distortions, w_m

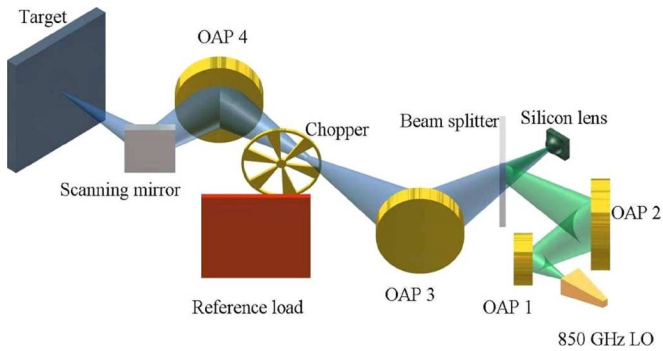


Fig. 6. Quasi-optical layout of the imaging system.

should be minimized by placing the mirrors close to the radiation source and, therefore, catching the beam before it expands significantly. Higher order modes were unavoidable due to space constraints in our design and resulted in optical beam distortions, which, in turn, degrade the imager spatial resolution.

The optical layout of the imaging system is illustrated in Fig. 6. OAP mirrors are arranged in such a way as to maximize the coupling efficiencies of both the LO and signal beams. The designed and measured beam sizes are plotted in Fig. 7(a) for the LO beam and Fig. 7(b) for the signal beam. All beam sizes are defined as twice the Gaussian beam radius w , where w is the radius at which the field is reduced by $1/e$ compared with the field on axis. The measured LO beam sizes agree with the theoretical prediction very well. In this case, the beam distortion was almost negligible and did not affect the LO biasing of the HEB device. Approximately 50% of OAP 1 and approximately 63% of OAP 2 were illuminated. However, the signal beam suffered strong distortions, especially at the focal planes of the different optical components along the horizontal direction [see Fig. 7(b)]. The focus blur (coma-type aberration) in our system is due to the higher order mode distortions, which can be estimated from (1). Similar strong coma aberrations were reported in other systems utilizing OAP mirrors [23], [24]. Slight misalignments of the mirrors can also contribute to such coma aberrations. Consequently, we were not able to focus the signal beam to the designed specification of slightly larger than 2 mm.

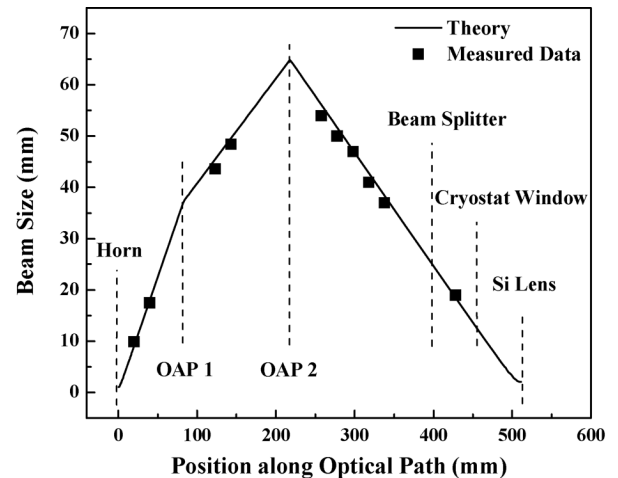
E. Postdetection Chain

The IF signal from the integrated receiver is further amplified with room-temperature amplifiers, having a total gain of approximately 60 dB. The IF bandwidth of the imaging system is fixed by an IF bandpass filter (1.3–3.5 GHz). The effective IF frequency band to be used in the radiometer equation [see (4)] is determined by the following equation [14]:

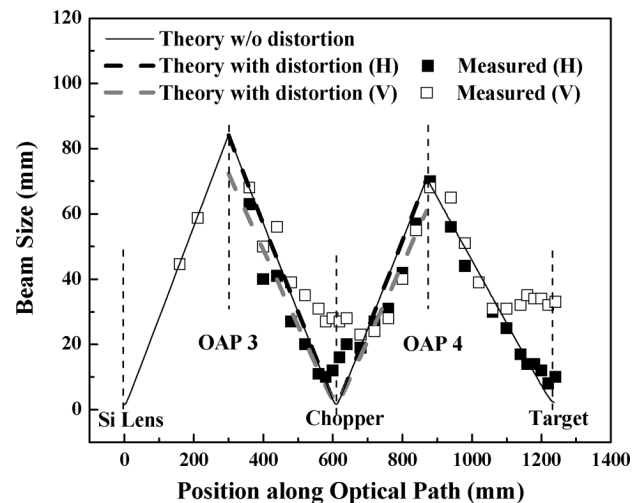
$$B_{\text{eff}} = T_{\text{RX}}^2(f = f_0) \cdot \int_{f_0}^{\infty} \frac{df}{T_{\text{RX}}^2(f)} \quad (3)$$

where f_0 is the lowest IF frequency (in our case, 0.5 GHz) at which the front-end receiver can produce low noise performance, and T_{RX} is a numerically fitted curve from the measured results of noise temperatures as a function of the IF frequency.

The optical chopper functions as a switch, delivering a modulated signal at a frequency (f_m) of 200 Hz. A zero-biased SBD is used to detect the IF power signal and convert it to a



(a)



(b)

Fig. 7. Theoretical and measured beam sizes (in diameter). (a) Along the optical path of the LO beam. (b) Along the horizontal and vertical direction of the signal beam.

dc signal. This SBD detector follows the square law detection for the input power level up to -15 dBm. A level of -20 dBm, corresponding to an output voltage at approximately 8 mV, was used. The output voltage signal is further amplified to approximately 1 V by use of an additional pre-amplifier. Next, a lock-in amplifier, referenced at the chopping frequency, is used. An integration time of 100 ms allows for the averaging of 20 signals at each pixel along the target.

F. Scanning Apparatus and DAQ

A 2-D scanning scheme was designed to record the image of the target by means of a line-by-line sweep, often called a raster scan. Each line of the scan is divided into a number of pixels. The number of pixels and the distance between pixels can be adjusted according to the desired resolution and the size of the target. The total wait period (dwell time) at each pixel has to be longer than the lock-in integration time constant. We set the dwell time to be three times longer than the lock-in integration time constant. An automated motion controller, which also functions as a DAQ system, is used to drive the translators and

TABLE I
IMAGING SYSTEM SPECIFICATIONS

Characteristics	Value
Receiver noise temperature (T_{RX})	1800 K
IF bandpass (B)	2.2 GHz
Total IF gain (G_{IF})	60 dB
Integration time on the lock-in amplifier (τ)	100 ms
Chopping speed (f_m)	200 Hz
Dwell time at each pixel (t_d)	300 ms
Typical scan time for a 40 by 40 pixel image	20 min

collect the data in real time.² The motion controller provides a 0.001° angular resolution and can gather data with 14-bit accuracy ($\pm 600 \mu\text{V}$ on a $\pm 10\text{-V}$ scale) at rates of up to 10 kHz. Such a setup allows the user to monitor the image quality in real-time. The scanning can be terminated and resumed at any time. A typical 40×40 pixel image takes approximately 20 min to complete. The movement of the translators contributes a significant portion of time to the total scan time.

The main specifications of our terahertz imaging system are summarized in Table I. The receiver noise temperature (T_{RX}) was measured using the standard Y -factor method. An optimization of the biasing conditions for both the HEB mixer and the LNA was carried out and plotted in Fig. 8. Each curve in Fig. 8(a) corresponds to a constant LO power, as estimated by the isothermal method [1], [12]. The lowest receiver noise temperature was achieved when the HEB was biased at 1.5 mV and 36 μA and the LNA's drain voltage was set at 1.6 V corresponding to a drain current of 16 mA. The total uncorrected effective noise temperature of the imager as measured at the target position (including optical losses due to the OAP mirrors, beam splitter, and free-space attenuation) was 1800 K. The effective IF bandwidth (B) was 2.2 GHz. Therefore, the theoretical imaging system sensitivity is given by the radiometer equation as follows:

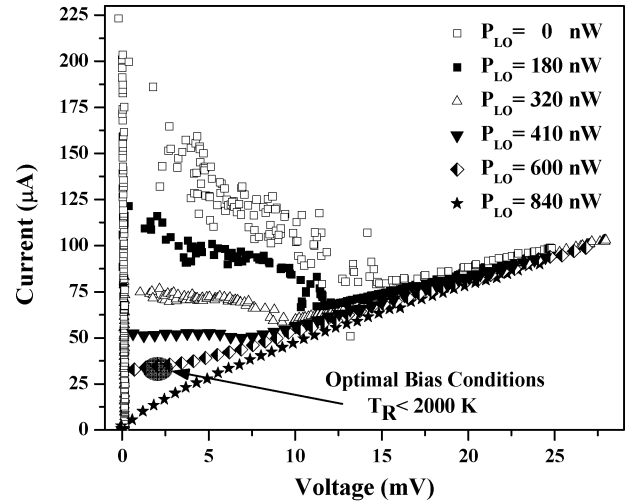
$$\Delta T_{\text{RMS}} = \frac{2 \cdot T_{\text{sys}}}{\sqrt{B \cdot \tau}} = \frac{2 \cdot (T_{\text{RX}} + 300 \text{ K})}{\sqrt{B \cdot \tau}} = 0.283 \text{ K}. \quad (4)$$

This theoretical prediction is the minimum temperature difference our imaging system can resolve and is also known as the noise equivalent temperature difference (NE ΔT) value. Here, we neglect the extra noise contribution due to the gain fluctuations (ΔG). To include gain fluctuations, (4) can be modified as follows [4]:

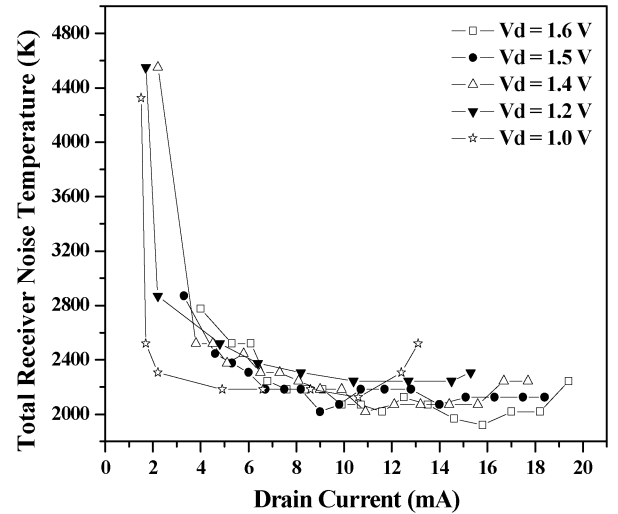
$$\Delta T_{\text{RMS}} = 2 \cdot T_{\text{sys}} \sqrt{\frac{1}{B \cdot \tau} + \left(\frac{\Delta G}{G}\right)^2}. \quad (5)$$

The gain fluctuation term is, in principle, negligible when using a Dicke receiver configuration, as long as the integration time is shorter than the characteristic time constant (the Allan time, discussed below) of the gain stability. The reference temperature should also be well matched to the target temperature, as it is in this case. Receiver noise temperature and bandwidth variations can also produce spurious output fluctuations. Therefore, the real imaging sensitivity is expected to be worse than the theoretical prediction (4).

²Newport Corporation, Irvine, CA.



(a)



(b)

Fig. 8. (a) I - V curves of a twin-slot antenna coupled HEB device. (b) Total receiver noise temperatures as a function of the LNA bias conditions.

IV. MEASURED PERFORMANCE OF THE HEB IMAGER

A. Imager Stability

The overall system stability is mainly determined by the short-term fluctuations of the front-end components. System noise includes uncorrelated noise (white noise) and correlated noise (flicker noise and drift noise). Different types of noise processes have different frequency dependencies and, therefore, different time constants. The Allan variance measurement is a practical method to characterize different types of noise processes in the time domain [25]. The Allan variance technique is widely adopted to characterize receivers used in astrophysical applications. The Allan time denotes the integration time when the overall noise is no longer produced by white noise and the correlated noise starts to dominate. As only white noise can be reduced by using the signal integration technique, the actual integration time is required to be set well below the Allan time.

The Allan variance measurements were carried out in a similar manner to that described in [26]. The HEB/LNA receiver was biased at its optimal operation point (maximum sensitivity)

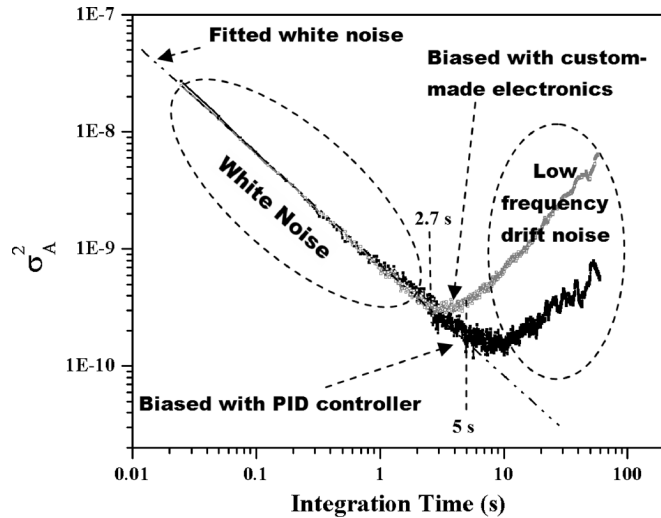


Fig. 9. Allan variance of the HEB/LNA receiver in a 1.3–3.5-GHz passband. The HEB is biased at the same points by using a commercial PID controller and a custom-made bias box.

and sensed the terahertz radiation from a black body at room temperature. The IF signal bandwidth is the same as the one used in the imaging system (1.3–3.5 GHz). A power meter is used to record the IF power as a function of time, keeping the temperature of the system very stable. The Allan time corresponds to the lowest value of the Allen variance plot. Fig. 9 shows the Allan variance plots for the receiver when the HEB device is dc biased with two different power sources. By replacing a custom-made dc bias box with a commercial low-noise proportional-integral-derivative (PID) controller, the Allan time was increased from 2.7 s to approximately 5 s. The Allan time for the entire system (the receiver plus the backend) is approximately 1.2 s. The Allan time of receiver systems based on HEB devices was reported to be less than 1 s by other groups [27]. The longer Allan time in our imaging system is attributed to a more stable harmonic multiplier LO source and a more stable dc-bias scheme by using the commercial PID controller. However, HEB mixers are, in general, less stable than SIS mixers, which typically produce an Allan time of approximately 10 s [26], [27]. The instability of the HEB is associated with the modulation of the width of the hot-spot region in the NbN bridge. Nevertheless, the shorter Allan time of HEB-based receivers does not present a limitation in imaging applications.

B. Imager Thermal Resolution

The overall imager thermal sensitivity is characterized by use of a voltage-biased heat blanket. The temperature of the blanket can be adjusted up to 40 K above room temperature and is measured with a calibrated thermocouple. Fig. 10(a) shows the resistor coil in front of a room-temperature absorber. Fig. 10(b) and (c) shows 850-GHz images of the resistor coil when the temperature differences are 35 and 1 K, respectively. The 1-K temperature difference image has some clutter due to noise in the system. A simple averaging filter is applied to post-process the image [see Fig. 10(d)]. The overall noise level is reduced and the 1-K temperature difference can be easily distinguished.

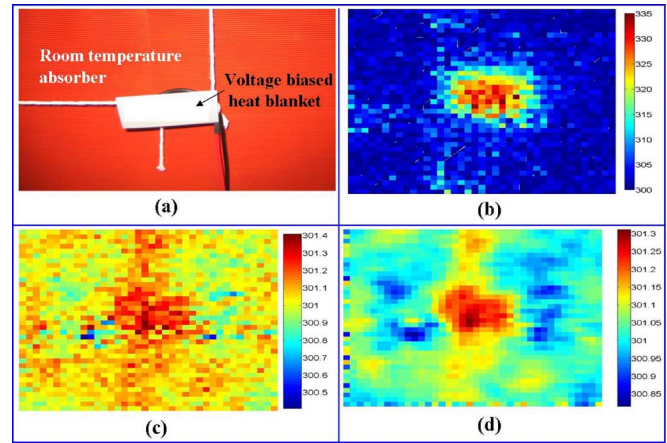


Fig. 10. (a) Voltage-biased heat blanket in front of the room-temperature absorber. 850-GHz images of the heat blanket with: (b) 35-K difference and (c) 1-K difference. (d) Post-processed image of the 1-K temperature difference image.

The image data are statistically analyzed to obtain the measured thermal sensitivity. The rms fluctuation is calculated to be 0.4 K ($\approx \sigma$) within a factor of 2 of the theoretical thermal sensitivity from (4).

C. Imager Spatial Resolution

The imaging spatial resolution is defined as the minimum distance between two point sources that can be distinguished by the imager. We used a ring-shaped absorber piece in order to characterize the imaging spatial resolution [see Fig. 11(a)]. The ring has inner and outer diameters of 16 and 26 mm. It is placed in front of a warm absorber, whose temperature is 5 K higher than the ring absorber. The 850-GHz image and the post-processed image are shown in Fig. 11(b) and (c), respectively. The ring appears to be distorted along the horizontal direction due to a more aggravated focus blur produced by the optical system. Quantitative analysis of the images shows that we can resolve structures as small as 4 mm.

V. DISCUSSION AND FUTURE DEVELOPMENTS

The results with this prototype imaging system have demonstrated the essential features to be expected of a future full-scale system that employs NbN HEB heterodyne detector elements. We achieved a measured resolvable temperature difference that is close to what is expected from theory. This level of sensitivity will be useful in practical systems. Gain fluctuations do not compromise the system sensitivity, as shown by the Allan variance study. Some aspects need to be improved and straightforward solutions appear feasible.

When used with a 90° deflection angle, OAPs can have surprisingly large aberrations, as shown in this study. This is an aspect that is not discussed much in the terahertz literature. OAPs with smaller deflection angles or dielectric lenses could be substituted.

The use of a mechanical chopper resulted in stable system performance and rapid progress toward a full-scale system. It is clear, however, that significant time delays occur by using a chopper, as discussed above. The next version of the system can easily cut down the current scan time of 1200 s for a 40 × 40

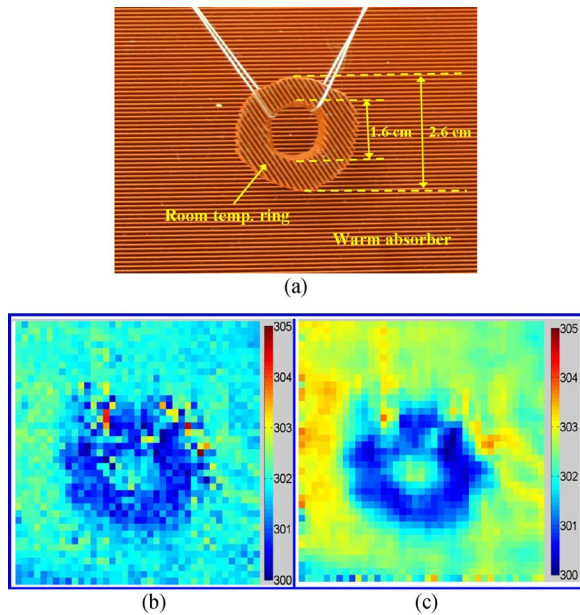


Fig. 11. (a) Photograph of a ring-shaped room-temperature absorber in front of a warm absorber (5-K difference). 850-GHz images of the object (b) original and (c) post-processed.

pixel image by a factor of approximately an order-of-magnitude (to 160 s) if the system is configured so that the effective dwell time on each pixel is approximately equal to the integration time. The same $NE\Delta T$ would be obtained. Calibration that assures gain stabilization can be built in by scanning reference loads at the edges of the target. The current motion controller is fast enough to allow this scan speed. Further improvements are possible in $NE\Delta T$ since the system noise temperature can be decreased to approximately 1000 K, while the effective IF bandwidth can be increased to as much as 8 GHz, as demonstrated in another recent HEB integrated receiver [28]. Using these values, we can decrease the integration time to 5 ms and achieve the same $NE\Delta T$, thus being able to scan the 40×40 pixel image in 8 s, a very practical imaging acquisition rate in medical imaging. Actual real-time imaging (say, 10–30 images/s) is also possible by employing an FPA of perhaps 100 elements. We demonstrated the first terahertz FPA (three elements at 1.6 THz) in [9].

By integrating heterodyne detectors in a specific configuration, significant sensitivity improvement can be achieved. An interferometer receiver consists of two or more heterodyne detectors with their antennas separated by a distance of a few wavelengths. The IF output voltages are added and detected, resulting in a system with an increased sensitivity (by a factor of 2) [4]. In a correlation receiver, the IF outputs are multiplied instead of added. The correlation receiver configuration improves the overall sensitivity by $2\sqrt{2}$ times over the Dicke receiver configuration. Moreover, gain instabilities will not affect the overall sensitivity of the system [4]. Different configurations of correlation receivers for the sub-millimeter-wave band are under development [29].

Finally, HEB heterodyne imaging can be combined with spectroscopy for identification and diagnostics of biological and chemical agents. A number of characteristic frequencies

can be sampled by tuning the LO and/or designing an array of HEB elements that detect these characteristic frequencies. Such multifrequency images with very high spectral resolution could be analyzed for identification of the different agents.

REFERENCES

- [1] E. Gerecht, C. Musante, Y. Zhuang, K. S. Yngvesson, T. Goyette, J. Dickinson, J. Waldman, P. Yagoubov, G. Gol'tsman, B. Voronov, and E. Gershenzon, "NbN hot electron bolometric mixers, a new technology for low-noise THz receivers," *IEEE Trans. Microw. Theory Tech.*, vol. 47, no. 12, pp. 2519–2527, Dec. 1999.
- [2] E. Gerecht *et al.*, "Deployment of TREND – A low noise receiver user instrument at 1.25 THz to 1.5 THz for AST/RO at the south pole," in *Proc. 14th Int. Space Terahertz Technol. Symp.*, Tucson, AZ, Apr. 2003, pp. 179–188.
- [3] R. Appleby and H. B. Wallace, "Standoff detection of weapons and contraband in the 100 GHz to 1 THz region," *IEEE Trans. Antennas Propag.*, vol. 55, no. 11, pp. 2944–2956, Nov. 2007.
- [4] J. D. Kraus, *Radio Astronomy*, 2nd ed. Durham, NH: Cygnus-Quasar Books, 1986.
- [5] M. Tiuri, "Radio astronomy receivers," *IEEE Trans. Antennas Propag.*, vol. AP-12, no. 7, pp. 930–938, Dec. 1964.
- [6] W. Bishop, T. Crowe, R. Mattauch, and H. Dossal, "Planar GaAs diodes for terahertz frequency mixing," in *Proc. 3rd Int. Space Terahertz Technol. Symp.*, Ann Arbor, MI, 1992, pp. 600–615.
- [7] R. J. Dengler, A. Skalare, and P. H. Siegel, "Passive and active imaging of humans for contraband detection at 640 GHz," in *Proc. IEEE MTT-S Int. Microw. Symp. Dig.*, Fort Worth, TX, Jun. 6–11, 2004, p. 1591.
- [8] J. C. Dickinson, T. M. Goyette, A. J. Gatesman, C. S. Joseph, Z. G. Root, R. H. Giles, J. Waldman, and W. E. Nixon, "Terahertz imaging of subjects with concealed weapons," *Proc. SPIE*, vol. 6212, pp. 1–12, 2006.
- [9] F. Rodriguez-Morales, K. S. Yngvesson, E. Gerecht, N. Wadefalk, J. Nicholson, D. Gu, X. Zhao, T. Goyette, and J. Waldman, "A terahertz focal plane array using HEB superconducting mixers and MMIC IF amplifiers," *IEEE Microw. Wireless Compon. Lett.*, vol. 15, no. 4, pp. 199–201, Apr. 2005.
- [10] R. Köhler, A. Tredicucci, F. Beltram, H. E. Beer, E. H. Linfield, A. G. Davies, D. A. Ritchie, R. C. Iotti, and F. Rossi, "Terahertz semiconductor-heterostructure laser," *Nature*, vol. 417, no. 6885, pp. 156–159, May 2002.
- [11] S. Cherednichenko, M. Kroug, P. Khosropanah, A. Adam, H. Merkel, E. Kollberg, D. Loudkov, B. Voronov, G. Gol'tsman, H.-W. Huebers, and H. Richter, "1.6 THz HEB mixer for far infrared space telescope (Herschel)," *Physica C*, vol. 372, pp. 427–431, Aug. 2002.
- [12] H. Ekström, B. Karasik, E. Kollberg, and K. S. Yngvesson, "Conversion gain and noise of niobium superconducting hot-electron mixers," *IEEE Trans. Microw. Theory Tech.*, vol. 43, no. 4, pp. 938–947, Apr. 1995.
- [13] H. Merkel, P. Khosropanah, and E. Kollberg, "A hot-spot mixer model for phonon-cooled NbN hot electron bolometric mixers," *IEEE Trans. Appl. Superconduct.*, vol. 9, no. 2, pp. 4201–4204, Jun. 1999.
- [14] F. Rodriguez-Morales, S. Yngvesson, R. Zannoni, E. Gerecht, D. Gu, N. Wadefalk, and J. Nicholson, "Development of integrated HEB/MMIC receivers for near-range terahertz imaging," *IEEE Trans. Microw. Theory Tech.*, vol. 54, no. 6, pp. 2301–2311, Jun. 2006.
- [15] S. Weinreb, "SIS mixer to HEMT amplifier optimum coupling network," *IEEE Trans. Microw. Theory Tech.*, vol. MTT-35, no. 11, pp. 1067–1069, Nov. 1987.
- [16] S. Padin, D. Woody, J. A. Stern, H. LeDuc, R. Blundell, C. Tong, and M. Pospieszalski, "An integrated SIS mixer and HEMT IF amplifier," *IEEE Trans. Microw. Theory Tech.*, vol. 44, no. 6, pp. 987–990, Jun. 1996.
- [17] V. P. Koshelets and S. V. Shitov, "Integrated superconducting receivers," *Supercond. Sci. Technol.*, vol. 13, pp. R53–R69, 2000.
- [18] C. Groppi, C. Walker, C. Kulesa, A. Hedden, P. Pütz, D. Golish, P. Gensheimer, C. D. d'Aubigny, S. Bussmann, S. Weinreb, G. Jones, J. Bardin, H. Mani, J. Kooi, G. Narayanan, A. Lichtenberger, and T. Kuiper, "SuperCam: A 64 pixel superheterodyne camera," in *Proc. 17th Int. Space Terahertz Technol. Symp.*, Paris, France, May 2006, pp. 323–326.
- [19] N. Wadefalk *et al.*, "Cryogenic wideband ultra-low-noise IF amplifiers operating at ultra-low DC power," *IEEE Trans. Microw. Theory Tech.*, vol. 51, no. 6, pp. 1705–1711, Jun. 2003.

- [20] J. Randa, E. Gerecht, D. Gu, and R. L. Billinger, "Precision measurement method for cryogenic amplifier noise temperatures below 5 K," *IEEE Trans. Microw. Theory Tech.*, vol. 54, no. 5, pp. 1180–1189, Mar. 2006.
- [21] D. F. Filipovic, S. S. Gearhart, and G. M. Rebeiz, "Double-slot antenna on extended hemispherical and elliptical silicon dielectric lenses," *IEEE Trans. Microw. Theory Tech.*, vol. 41, no. 10, pp. 1738–1749, Oct. 1993.
- [22] P. F. Goldsmith, *Quasioptical Systems*. New York: Wiley, 1997.
- [23] M. A. Lieb and A. J. Meixner, "A high numerical aperture parabolic mirror as imaging device for confocal microscopy," *Opt. Exp.*, vol. 8, no. 7, pp. 458–474, 2001.
- [24] C. J. R. Sheppard, "Aberrations in high aperture optical systems," *Optik*, vol. 105, pp. 29–33, 1997.
- [25] D. W. Allan, "Statistics of atomic frequency standards," *Proc. IEEE*, vol. 54, no. 2, pp. 221–230, Feb. 1966.
- [26] J. W. Kooi, J. A. Baselmans, A. Baryshev, R. Schieder, M. Hajenius, J. R. Gao, T. M. Klapwijk, B. Voronov, and G. Gol'tsman, "Stability of heterodyne terahertz receivers," *J. Appl. Phys.*, vol. 100, no. 6, 2006, 064904.
- [27] T. Berg, S. Cherednichenko, V. Drakinskiy, P. Khosropanah, H. Merkel, E. Kollberg, and J. W. Kooi, "Stability of HEB receiver at THz frequencies," *Proc. SPIE*, vol. 5498, pp. 605–615, 2004.
- [28] F. Rodríguez-Morales, S. Yngvesson, D. Gu, N. Wadefalk, K. Fu, C. Chan, J. Nicholson, and E. Gerecht, "Highly packaged HEB receivers using three-dimensional integration," in *Proc. 18th Int. Space Terahertz Technol. Symp.*, Pasadena, CA, Mar. 21–23, 2007.
- [29] A. Navarrini and M. Carter, "Design of a dual polarization SIS sideband separating receiver based on waveguide OMT for the 275–370 GHz frequency band," in *Proc. 14th Int. Space Terahertz Technol. Symp.*, Tucson, AZ, Apr. 2003, pp. 159–168.



Eyal Gerecht (S'88–M'97) received the B.S.E.E. degree in electrical engineering with a minor in solid-state physics (*magna cum laude*) from the University of Houston, Houston, TX, in 1990, and the M.S.E.C.E. and Ph.D. degrees in electrical and computer engineering from the University of Massachusetts at Amherst, in 1994 and 1998, respectively.

In 1998, he joined the Department of Physics and Astronomy, University of Massachusetts at Amherst, as a Senior Postdoctoral Research Associate. Since 2000, he has been a Physicist with the Electro-

magnetics Division, National Institute of Standards and Technology (NIST), Boulder, CO, where he develops a number of terahertz-related technologies.



Dazhen Gu (S'01) received the B.S. degree in physics from Nanjing University, Nanjing, China, in 1999, and the M.S.E.C.E and Ph.D. degrees in electrical and computer engineering from the University of Massachusetts at Amherst, in 2004 and 2007, respectively.

From 1999 to 2001, he was a Research Assistant with the Superconductor Electronics Laboratory, Nanjing University. Since 2001, he has been involved in the design and fabrication of NbN hot electron bolometric mixers for terahertz receivers.

Since November 2003, he has been with the Electromagnetics Division, National Institute of Standards and Technology (NIST), Boulder, CO.



Lixing You received the B.S., M.S., and Ph.D. degrees in physics from Nanjing University, Nanjing, China, in 1997, 2001, and 2003, respectively.

From 2003 to 2005, he was a Post-Doctoral Researcher with the Department of Microtechnology and Nanoscience (MC2), Chalmers University of Technology, Göteborg, Sweden. From 2005 to 2006, he was a Post-Doctoral Researcher with the Condensed Matter Physics and Devices Group, University of Twente, Twente, The Netherlands. Since 2006, he has been a Guest Researcher with

the Electromagnetics Division, National Institute of Standards and Technology (NIST), Boulder, CO, where he is engaged in the development of terahertz imaging and spectroscopy with HEB technology.



K. Sigfrid Yngvesson (M'62–SM'92–F'98–LF'02) received the Civilingenjör degree and Tekn. Dr. degree in electrical engineering from the Chalmers University of Technology, Göteborg, Sweden, in 1958 and 1968, respectively.

From 1968 to 1970, he was a Post-Doctoral Fellow with the University of California at Berkeley. Since 1970, he has taught at the University of Massachusetts at Amherst, becoming a Full Professor in 1978. He authored *Microwave Semiconductor Devices* (Kluwer, 1991). He has been involved with maser

low-noise receivers for radio astronomy and integrated antenna arrays. His current research interests are terahertz low-noise devices and applications, in particular, hot electron bolometric mixers and FPA's, and terahertz applications of carbon nanotubes.